Measurement of nuclear excitation functions for proton induced reactions (E_p = 40 – 90 MeV) on Nb and Cu

Andrew S. Voyles[a,*], Lee A. Bernstein[a,b], Eva R. Birnbaum[d], Jonathan W. Engle[c],
Stephen A. Graves[e], Amanda M. Lewis[a], Francois M. Nortier[d]

[a]Department of Nuclear Engineering, University of California, Berkeley, 4155 Etcheverry Hall, MC 1730, Berkeley, CA 94720,
USA
[b]Lawrence Berkeley National Laboratory, 1 Cyclotron Rd., Berkeley, CA 94720, USA
[c]Department of Medical Physics, University of Wisconsin – Madison, 1111 Highland Ave., Madison, WI 53705, USA
[d]Los Alamos National Laboratory, P.O. Box 1663, Los Alamos, NM 87544, USA
[e]Department of Radiation Oncology, University of Iowa, 200 Hawkins Drive, Iowa City, IA 52242, USA

Abstract

XXXXX

Keywords: Nb+p, Cu+p, Niobium, Copper, Aluminum, Nuclear cross sections, Proton activation, Proton transport, Stacked target activation, Monitor foils, Medical isotope production, MCNP, LANL

Todo list

1. Introduction

Every year, approximately 17 million nuclear medicine procedures (both diagnostic and therapeutic) are performed in the U.S. alone - a multi-billion dollar industry which has made incredible strides in improving our ability to detect and treat a variety of life-threatening diseases [1, 2]. The vast majority of the radioisotopes currently used for these procedures are produced in the field's array of low- (E < 30 MeV / A) and intermediate-energy (30 < E < 200 MeV / A) accelerator capabilities, which routinely produce many of the staple medical radionuclides, such as ^{18}F ^{68}Ge, ^{82}Rb, and ^{123}I, as well as many of the non-medical radioisotopes of commercial value, such as ^{32}Si, ^{73}As, ^{95m}Tc, and ^{109}Cd [3, 4].

---

*Corresponding author
Email address: andrew.voyles@berkeley.edu (Andrew S. Voyles)

ASV: Should "intermediate-energy" be less than 200 MeV, or 100 MeV? I find conflicting descriptions in the literature.

The future of nuclear medicine would appear to be the paradigm of personalized medicine - targeted radionuclide therapy to spare healthy tissue [5, 6], and theranostic medicine, which pairs an imaging isotope with a therapeutic isotope of the same element, to provide simultaneous, real-time dose delivery and verification, leading to drastic reductions in prescribed patient dose [7, 8, 9]. Candidate isotopes to fill these needs have been identified based on their decay properties [2, 6, 10], and a series of campaigns are underway to perform targeted, high-priority measurements of thin-target cross sections and thick-target integral yields, to facilitate production in sufficient quantities for cell studies.

However, one significant obstacle exists for both high-fidelity measurements of emerging medical radionuclides, as well as conventional isotope production: well-characterized dosimetry standards. This is particularly true for intermediate-energy charged particle beams, where there is currently a paucity of such well-characterized data. Indeed, the development of new dosimetry standards and the improved evaluation of existing standards is one of the areas of greatest cross-cutting need for nuclear data [10]. Charged particle dosimetry data currently exists for low-to-intermediate energy charged particle beams (E < 50 MeV / A), but experimental data used for this evaluation is sparse above approximately 30 MeV / A and uncertainties in experimental cross sections are large (6-15%) [11]. While work is needed to improve upon existing dosimetry data, the development of new dosimetry reactions can expand the available range of options for the monitoring of charged particle beams.

Activation is one of the most fundamental techniques utilized in experimental nuclear physics, as it is a simple and straightforward method to probe the structure and behavior of nuclear matter, dating back to the infancy of the field. While the specifics have branched into ever-more-detailed probes into the world of the nucleus, activation, at heart, deals with the analysis and quantification of decaying radioactive nuclei created through irradiation via ionizing radiation [12, 13]. Monitor reactions have historically been part of such activation experiments, and in the context of charged particle induced reactions, serve two valuable purposes, depending upon the energy regime in question. Between the reaction's energetic threshold and the tail of its compound peak, the magnitude and shape of a monitor reaction's excitation function is rapidly changing with increasing incident particle energy. In this energy regime, a monitor reaction can be used to assign an energy bin to a thin irradiated target, especially when comparing between monitor reactions leading to two distinct residual nuclei from the same target, such as the $^{nat}Cu(p,x)^{62}Zn$ and $^{nat}Cu(p,x)^{63}Zn$ reactions [11]. This is extremely useful, as it allows one to screen for and eliminate systematic errors based on energy assignment, though this sensitivity to energy precludes their reliability as a beam current monitor.

Moving to the higher energy of the reaction's pre-equilibrium tail, the excitation function becomes smooth and generally flat as a function of energy. In this regime, the monitor reaction offers little-to-no energy sensitivity. In return for giving up the ability to assign energy positions, monitor reactions in the pre-equilibrium regime become extremely useful for monitoring the integral beam current incident upon the target. While cross section measurements often use external beam current monitors (such as an inductive pickup upstream of a target, or electrically-isolated target in a Faraday cup), these measure the integrated current incident upon an entire target assembly. For the case of stacked-target activation experiments, commonly employed to measure cross sections at multiple energy positions in a single activation, external beam current monitors can only measure the integral current incident upon the "front" (upstream) of the target stack. In these experiments, a series of monitor foils at each energy position allow one to measure the integral current at each position in the stack, reducing systematic errors in observed cross section magnitude. Both of these purposes make well-characterized dosimetry an invaluable asset to any activation experiment.

In practice, nearly any radioisotope can serve as a reaction monitor. However, several characteristics are hallmarks of a reaction monitor worthy to be classified as a dosimetry standard. The primary factor involved in selecting a new monitor is ensuring that the desired radionuclide has at least one (preferably multiple, to ensure accurate radionuclide identification) distinct decay radiation able to used to uniquely identify it during post-activation assay. Generally, this means selecting a radionuclide with a number of distinct gamma rays, as gamma spectroscopy is commonly used to identify and quantify reaction products. The decay radiation should preferably have high intensities, so that they show up as strong peaks during

spectroscopy, and minimize the amount of time needed to count the activated target in order to achieve acceptable counting statistics.

Care should be taken to avoid cases where a radionuclide which is one decay off of stability populates excited states in the excited daughter nucleus also populated in the decay to the daughter state from the opposite side of the valley of stability. This produces decay gamma rays with nearly exactly the same energy, making it difficult to disentangle production from both sides of stability. For example, ^{nat}Ti(p,x)^{48}V is commonly used as dosimetry for $5 < E < 30$ MeV protons. The characteristic decay lines in ^{48}V ($t_{1/2} = 15.97$ d, $\epsilon = 100\%$ to ^{48}Ti) are the 983.525 keV ($I_\gamma = 99.98\%$) and 1312.106 keV ($I_\gamma = 98.2\%$) gammas, which are also seen in the decay of ^{48}Sc ($t_{1/2} = 43.67$ h, $\beta^- = 100\%$ to ^{48}Ti), yielding a 983.526 keV ($I_\gamma = 100.1\%$) and 1312.120 keV ($I_\gamma = 100.1\%$) line [14]. Fortunately, these cases can occasionally be mitigated by either using a difference in half-life between the two feeding pathways to allow one to decay out, or by using a distinct gamma ray from one of the two isobar nuclei to subtract out the activity associated with it (such as the $E_\gamma = 1037.522$ keV, $I_\gamma = 97.6\%$ line in the decay of ^{48}Ti) [14]. However, this approach propagates larger uncertainties into the final activity of the desired monitor nucleus, so in principle it is far preferred to choose a monitor reaction which does not have overlapping gamma rays from another isobar nucleus.

Another important decay factor to consider is that of the half-life of the desired monitor nucleus. It is preferred that the nucleus have a lifetime which is sufficiently long-lived to ensure that it may be quantified conveniently and leisurely after end-of-beam without the majority if it decaying away. In addition, it is preferred that the lifetime be comparable to that of the reaction products being studied. For proper quantification, it is also of vital importance that the proposed monitor nucleus have well-characterized decay data. A precise and well-established half-life is needed to properly correct for decay losses during production, as well as in between end-of-beam and the start of decay spectroscopy, but these are generally well-characterized. In practice, the weakest components of decay data are often the gamma ray intensities, which can routinely have uncertainties of 5% or more. Since this uncertainty is propagated in quadrature from the activity of both the monitor reaction and the reaction product being studied, choosing a monitor with a well-established gamma ray intensity can make a significant reduction in measured cross section uncertainties. It is also of utmost importance to choose a reaction channel which cannot be populated via secondary particles incident upon the monitor target. This is typically mostly a concern for secondary neutrons produced through (z,xn) reactions on upstream targets, degraders, and stack materials, to avoid monitor reactions which can be populated through (n,x) reactions on the target. Any monitor reaction channel which can be populated by anything other than the primary beam should be avoided, as it is often a laborious task to separate out the fraction of secondary particles contributing to the total activation.

Finally, from a targetry perspective, it is preferable to use a target that is readily commercially available at an affordable price and is generally chemically inert - any significant chemical changes during target preparation (rapid oxidation, etc) will affect the target's areal density, systematically changing the measured integral current. Structurally, the target material should be malleable and supportive to be able to be formed into a thin target. For charged particle reactions, a thin target is desired for dosimetry, as thicker targets will cause more energy degradation and broaden the energy spectrum downstream of the target.

One monitor reaction which satisfies these requirements is that of a new, intermediate-energy proton dosimetry standard based on ^{93}Nb(p,4n)^{90}Mo. Niobium is naturally monoisotopic, readily available commercially in high purity, is chemically inert, and can easily be rolled down to foils as thin as 1 µm. ^{90}Mo also has excellent decay properties - its fairly long-lived half-life ($\epsilon = 100\%$, $t_{1/2} = 5.56 \pm 0.09$ h) allows it to be counted at leisure without fear of the product ^{90}Mo decaying away excessively between end-of-beam and the start of counting, and it possesses seven strong, distinct gamma lines (notably its 122.370 keV ($I_\gamma = 64 \pm 3\%$) and 257.34 keV ($I_\gamma = 78 \pm 4\%$) lines) which can be used to uniquely and easily quantify ^{90}Mo production [15]. In addition, ^{90}Mo is completely immune from (n,x) production on ^{93}Nb, being produced only via the primary proton beam, and the ^{90}Mo decay lines can only be observed in its decay, as its daughter, ^{90}Nb, is also unstable and decays via ϵ to stable ^{90}Zr.

The purpose of the present work is to measure the production of the long-lived radionuclide ^{90}Mo ($t_{1/2} = 5.56 \pm 0.09$ h [15]) via the ^{nat}Nb(p,x) reaction. In addition to the ^{nat}Nb(p,x)^{90}Mo measurement, this experiment has also yielded measurements of 32 other (p,x) production cross sections between $40 - 90$ MeV for a number of additional reaction products, including several emerging radionuclides with medical applications.

These include the non-standard positron emission tomography (PET) emitters ^{57}Ni ($t_{1/2} = 35.60 \pm 0.06$ h [16]), ^{86}Y ($t_{1/2} = 14.74 \pm 0.02$ h [17]), ^{89}Zr ($t_{1/2} = 78.41 \pm 0.12$ h [18]), ^{90}Nb ($t_{1/2} = 14.60 \pm 0.05$ h [15]), the β^--therapy agent ^{64}Cu ($t_{1/2} = 12.701 \pm 0.002$ h [19]), and the Auger-therapy agent ^{82m}Rb ($t_{1/2} = 6.472 \pm 0.006$ h [20]).

> ASV: The following paragraph should only be included if we decide to touch on spin physics in this manuscript, or split it into a follow-on PhysRev C, etc.

Measurements of isomer-to-ground state ratios have been used for over 20 years to probe the spin distribution of excited nuclear states in the A$\approx$ 190 region [21, 22]. In addition to the interest in the production of ^{90}Mo as an intermediate-energy dosimetry standard, this experiment offers an opportunity to study the distribution of angular momentum in compound nuclear and direct pre-equilibrium reactions via observation of a number of isomer-to-ground state ratios. These include the ^{52m}Mn ($t_{1/2} = 21.1 \pm 0.2$ m; J$^\pi = 2^+$) to ^{52g}Mn ($t_{1/2} = 5.591 \pm 0.003$ d; J$^\pi = 6^+$), ^{58m}Co ($t_{1/2} = 9.10 \pm 0.09$ h; J$^\pi = 5^+$) to ^{58g}Co ($t_{1/2} = 70.86 \pm 0.06$ d; J$^\pi = 2^+$), ^{85m}Y ($t_{1/2} = 4.86 \pm 0.13$ h; J$^\pi = 9/2^+$) to ^{85g}Y ($t_{1/2} = 2.68 \pm 0.05$ h; J$^\pi = 1/2^-$), ^{87m}Y ($t_{1/2} = 13.37 \pm 0.03$ h; J$^\pi = 9/2^+$) to ^{87g}Y ($t_{1/2} = 79.8 \pm 0.3$ h; J$^\pi = 1/2^-$), and ^{89m}Nb ($t_{1/2} = 66 \pm 2$ m; J$^\pi = 1/2^-$) to ^{89g}Nb ($t_{1/2} = 2.03 \pm 0.07$ h; J$^\pi = 9/2^+$) ratios [23, 24, 25, 26, 18].

This measurement has taken place using a set of multiple monitor reactions in conjunction with statistical calculations and proton transport simulations to reduce systematic uncertainties in beam energy assignments, leading to some of the first and most precise measurements for many of the excitation functions reported here. By expanding the available set of dosimetry standards and well-characterized isotope production excitation functions, great advances are possible for improving the available options for modern medical imaging and cancer therapy.

2. Experimental methods and materials

2.1. Stacked-target design

The well-known stacked-target design was utilized for this work, in order that the (p,x) cross sections for each reaction channel could be measured at multiple energy positions in a single irradiation [27]. For targets, a series of nominal 25 μm ^{nat}Nb foils (99.8%, lot #T23A035), 25 μm ^{nat}Al foils (99.999%, lot #M06C032), and 50 μm ^{nat}Cu foils (99.9999%, lot #N26B062) were used (all from Alfa Aesar, Ward Hill, MA, 01835, USA). Six foils of each metal were cut down to 2.5 x 2.5 cm squares and characterized - for each foil, length and width measurements were taken at four different locations using a Mitutoyo caliper, thickness measurements were taken at four different locations using a Mitutoyo micrometer, and four mass measurements were taken using an analytical balance after cleaning the foils with isopropyl alcohol. Using these length, width, and mass readings, the areal density (in mg/cm^2) for each foil was calculated, along with the propagated uncertainty in areal density. The foils were tightly sealed into "packets" using two pieces of 3M 5413-Series Kapton polyimide film tape - each piece of tape consists of 43.2 μm of a silicone adhesive on 25.4 μm of a polyimide backing. The sealed foils were mounted over the hollow center of a 1.575 mm-thick plastic frame, and one ^{nat}Al, one ^{nat}Cu, and ^{nat}Nb mounted foil were bundled together using baling wire for each energy position. These foil packet bundles were lowered into the beam line by inserting them into a water-cooled production target box. The box, seen in Figure 1, is machined from 6061 aluminum alloy, has a thin (0.64 mm) Inconel beam entrance window, and contains 6 "energy positions" for targets, formed by 5 slabs of 6061 aluminum alloy (previously characterized) which serve as proton energy degraders between energy positions. At both the front and rear of the target stack's foils, a 316 stainless steel foil is inserted to serve as a beam profile monitor - after end-of-beam (EoB), β particles emitted from these activated stainless steel foils may be used to develop Gafchromic film, revealing the spatial profile of the beam entering and exiting the stack. After loading all targets in the stack, the lid of the target box is sealed in place, using an inset o-ring to create a water-tight seal, and the box is lowered through a hot cell into the beamline, where it sits electrically isolated. The specifications of the target stack design for this work is presented in Table 1.

> ASV: Confirm beam parameters below, from notebook

157   This target stack was assembled and irradiated at the Isotope Production Facility (IPF) at the Los
158 Alamos National Laboratory (LANL), using the LANSCE linear accelerator. The stack was irradiated for
159 approximately 2 hours with a nominal current of 1 mA, using a 100 μs pulse at a frequency of 1 Hz, for an
160 anticipated integral current of 205.9 nAh. The proton beam incident upon the stack's Inconel beam entrance
161 window had a calculated energy of 100 MeV, with an approximately Gaussian energy distribution width of 0.1
162 MeV - this energy profile was used for all later analysis. At the end of the irradiation, the target stack was
163 withdrawn from the beamline into the IPF hot cell, where it was disassembled and the activated foils removed
164 using robotic manipulators. The activated foils were cleaned of all surface contamination, and transported to
165 a counting lab for decay spectroscopy, which started approximately 7 hours following end-of-beam.
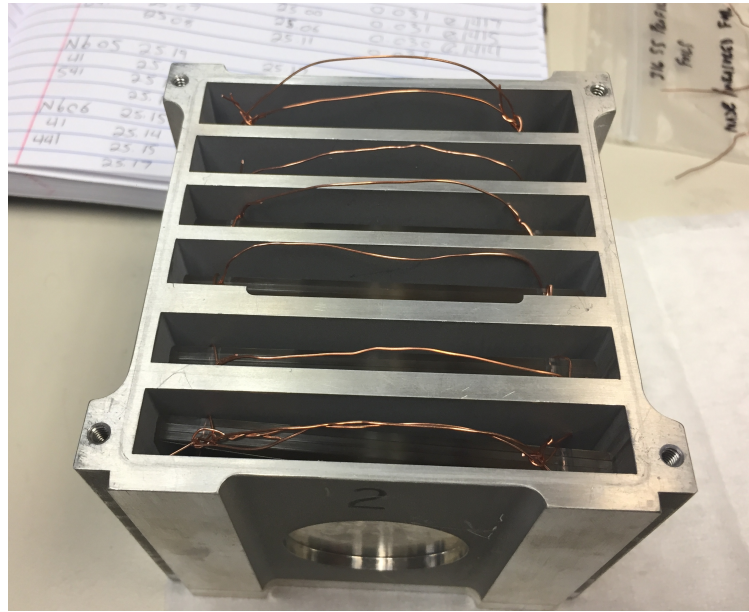

Figure 1. Photograph of the assembled IPF target stack, before the stack's o-ring lid was sealed in place. The baling wire handles affixed to each bunch of Al+Cu+Nb foils are visible in each energy position, to facilitate removal of activated foils via robotic manipulators in the IPF hot cell. The circular Inconel beam entrance aperture is visible in the bottom center of the photograph.

166 *2.2. Measurement of induced activities*

167   XXXXXX

168 *2.3. Proton dosimetry*

169   XXXXXX

170 *2.4. Proton transport calculations*

171   XXXXXX

172 *2.5. Calculation of measured cross sections*

173   XXXXXX

174 *2.6. Systematic uncertainties*

175   XXXXXX

Table 1. Specifications of the target stack design in the present work. The proton beam enters the stack upstream of the 249.8 µm SS profile monitor, and is transported through the stack in the order presented here. The 6061 aluminum degraders have a measured density of approximately 2.80 g/cm^3, but their areal densities are not listed here due to the variance minimization techniques described in this work.

Target layer	Measured thickness	Measured areal density (mg/cm^2)	Areal density uncertainty (%)
SS profile monitor	249.8 µm	194.555	0.290
Al-1	25.0 µm	6.519	0.724
Cu-1	61.3 µm	53.736	0.053
Nb-1	30.0 µm	23.205	0.073
Al Degrader 01	4.96 mm	-	-
Al-2	25.5 µm	6.484	0.364
Cu-2	61.8 µm	53.849	0.169
Nb-2	30.8 µm	22.905	0.166
Al Degrader 02	4.55 mm	-	-
Al-3	25.8 µm	6.472	0.314
Cu-3	61.5 µm	53.984	0.113
Nb-3	31.0 µm	22.906	0.235
Al Degrader 03	3.52 mm	-	-
Al-4	26.3 µm	6.505	0.407
Cu-4	61.3 µm	53.463	0.221
Nb-4	30.8 µm	22.550	0.245
Al Degrader 04	3.47 mm	-	-
Al-5	26.5 µm	6.479	0.296
Cu-5	61.5 µm	53.572	0.108
Nb-5	30.8 µm	22.110	0.248
Al Degrader 05	3.46 mm	-	-
Al-6	26.3 µm	6.475	0.624
Cu-6	62.0 µm	53.836	0.318
Nb-6	31.3 µm	22.120	0.130
SS profile monitor	124.4 µm	101.336	0.226

3. Results

XXXXXX

4. Conclusions

XXXXXX

5. Acknowledgements

Appendix A. Decay data

Table of decay data used for observed gamma rays.

Appendix B. Measured excitation functions

Plots of the cross sections measured in this work are presented here, in comparison with literature data and reaction modeling codes.

References

[1] D. Delbeke, G. M. Segall, Status of and Trends in Nuclear Medicine in the United States, Journal of Nuclear Medicine 52 (Supplement 2) (2011) 24S–28S. `doi:10.2967/jnumed.110.085688`.

[2] NSAC Isotopes Subcommittee, Meeting Isotope Needs and Capturing Opportunities for the Future: The 2015 Long Range Plan for the DOE-NP Isotope Program, Tech. rep. (2015).

[3] International Atomic Energy Agency, Cyclotron Produced Radionuclides: Physical Characteristics and Production Methods, no. 468 in Technical Reports Series, INTERNATIONAL ATOMIC ENERGY AGENCY, Vienna, 2009.

[4] D. J. Schlyer, P. den Winkel, T. J. Ruth, M. M. Vora, M. Pillai, M. Haji-Saeid, Cyclotron produced radionuclides: Principles and practice, Tech. Rep. 465, Technical Reports Series (2008).

[5] D. A. Mulford, D. A. Scheinberg, J. G. Jurcic, The Promise of Targeted α-Particle Therapy, Journal of Nuclear Medicine 46 (1 suppl) (2005) 199S–204S.

[6] S. M. Qaim, Nuclear data for production and medical application of radionuclides: Present status and future needs, Nuclear Medicine and Biology 44 (2016) 31–49. `doi:10.1016/j.nucmedbio.2016.08.016`.

[7] C. Müller, M. Bunka, S. Haller, U. Köster, V. Groehn, P. Bernhardt, N. van der Meulen, A. Türler, R. Schibli, Promising Prospects for 44Sc-/47Sc-Based Theragnostics: Application of 47Sc for Radionuclide Tumor Therapy in Mice, Journal of Nuclear Medicine 55 (10) (2014) 1658–1664. `doi:10.2967/jnumed.114.141614`.

[8] S. M. Bentzen, Theragnostic imaging for radiation oncology: dose-painting by numbers, The Lancet Oncology 6 (2) (2005) 112–117. `doi:10.1016/S1470-2045(05)01737-7`.

[9] S. C. Srivastava, Paving the Way to Personalized Medicine: Production of Some Promising Theragnostic Radionuclides at Brookhaven National Laboratory, Seminars in Nuclear Medicine 42 (3) (2012) 151–163. `doi:10.1053/j.semnuclmed.2011.12.004`.

[10] L. A. Bernstein, D. Brown, A. M. Hurst, J. H. Kelley, F. G. Kondev, E. A. McCutchan, C. D. Nesaraja, R. Slaybaugh, A. Sonzogni, Nuclear Data Needs and Capabilities for Applications Whitepaper, Tech. rep., Lawrence Livermore National Laboratory (LLNL), Livermore (2015).

[11] S. Qaim, F. Tárkányi, P. Oblozinsky, K. Gul, A. Hermanne, M. Mustafa, F. Nortier, B. Scholten, Y. Shubin, S. Takács, Y. Zhuang, Charged particle cross-section database for medical radioisotope production: diagnostic radioisotopes and monitor reactions, IAEA-TECDOC-1211.

[12] W. D. Ehmann, D. E. Vance, Radiochemistry and Nuclear Methods of Analysis, Chemical Analysis: A Series of Monographs on Analytical Chemistry and Its Applications, Wiley, 1993.

[13] P. Krüger, Principles of activation analysis, Wiley-Interscience, 1971.

[14] T. W. Burrows, Nuclear Data Sheets for A = 48, Nuclear Data Sheets 107 (7) (2006) 1747–1922. `doi:10.1016/j.nds.2006.05.005`.

[15] E. Browne, Nuclear Data Sheets for A = 90, Nuclear Data Sheets 82 (3) (1997) 379–546. `doi:10.1006/ndsh.1997.0021`.

[16] M. R. Bhat, Nuclear Data Sheets for A = 57, Nuclear Data Sheets 85 (3) (1998) 415–536. `doi:10.1006/ndsh.1998.0021`.

[17] A. Negret, B. Singh, Nuclear Data Sheets for A = 86, Nuclear Data Sheets 124 (2015) 1–156. `doi:10.1016/j.nds.2014.12.045`.

[18] B. Singh, Nuclear Data Sheets for A = 89, Nuclear Data Sheets 114 (1) (2013) 1–208. `doi:10.1016/j.nds.2013.01.001`.

[19] B. Singh, Nuclear Data Sheets for A = 64, Nuclear Data Sheets 108 (2) (2007) 197–364. `doi:10.1016/j.nds.2007.01.003`.

[20] J. Tuli, Nuclear Data Sheets for A = 82, Nuclear Data Sheets 98 (2) (2003) 209–334. `doi:10.1006/ndsh.2003.0002`.

[21] S. Sudár, S. M. Qaim, Cross sections for the formation of ^{195}Hg^{m,g}, ^{197}Hg^{m,g}, and ^{196}Au^{m,g} in α and ^{3}He-particle induced reactions on Pt: Effect of level density parameters on the ca, Phys. Rev. C 73 (3) (2006) 34613. `doi:10.1103/PhysRevC.73.034613`.

[22] N. Chakravarty, P. K. Sarkar, S. Ghosh, Pre-equilibrium emission effects in the measured isomeric yield ratios in alpha-induced reactions on ^{197}Au, Phys. Rev. C 45 (3) (1992) 1171–1188. `doi:10.1103/PhysRevC.45.1171`.

[23] Y. Dong, H. Junde, Nuclear Data Sheets for A = 52, Nuclear Data Sheets 128 (2015) 185–314. `doi:10.1016/j.nds.2015.08.003`.

[24] C. D. Nesaraja, S. D. Geraedts, B. Singh, Nuclear Data Sheets for A = 58, Nuclear Data Sheets 111 (4) (2010) 897–1092. `doi:10.1016/j.nds.2010.03.003`.

[25] B. Singh, J. Chen, Nuclear Data Sheets for A = 85, Nuclear Data Sheets 116 (Supplement C) (2014) 1–162. `doi:10.1016/j.nds.2014.01.001`.

[26] T. D. Johnson, W. D. Kulp, Nuclear Data Sheets for A = 87, Nuclear Data Sheets 129 (2015) 1–190. `doi:10.1016/j.nds.2015.09.001`.

[27] S. A. Graves, P. A. Ellison, T. E. Barnhart, H. F. Valdovinos, E. R. Birnbaum, F. M. Nortier, R. J. Nickles, J. W. Engle, Nuclear excitation functions of proton-induced reactions (Ep=35-90 MeV) from Fe, Cu, and Al, Nuclear Instruments and Methods in Physics Research, Section B: Beam Interactions with Materials and Atoms 386 (2016) 44–53. `doi:10.1016/j.nimb.2016.09.018`.